Acta Crystallographica Section A
Foundations of Crystallography
ISSN 0108-7673

Received 8 June 2009
Accepted 12 October 2009

Reconstruction from a single diffraction pattern of azimuthally projected electron density of molecules aligned parallel to a single axis

D. K. Saldin,[a]* V. L. Shneerson,[a] D. Starodub[b] and J. C. H. Spence[b]

[a]Department of Physics, University of Wisconsin–Milwaukee, PO Box 413, Milwaukee, WI 53201, USA, and [b]Department of Physics, Arizona State University, Tempe, AZ 85287, USA. Correspondence e-mail: dksaldin@uwm.edu

Diffraction from the individual molecules of a molecular beam, aligned parallel to a single axis by a strong electric field or other means, has been proposed as a means of structure determination of individual molecules. As in fiber diffraction, all the information extractable is contained in a diffraction pattern from incidence of the diffracting beam normal to the molecular alignment axis. The limited size of the object results in continuous diffraction patterns characterized by neither Bragg spots nor layer lines. Equations relating the scattered amplitudes to the molecular electron density may be conveniently formulated in terms of cylindrical harmonics. For simulated diffraction patterns from short C nanotubes aligned along their axes, iterative solution of the equation for the zeroth-order cylindrical harmonic and its inverse with appropriate constraints in real and reciprocal space enables the phasing of the measured amplitudes, and hence a reconstruction of the azimuthal projection of the molecule.

1. Introduction

Perhaps the most famous diffraction pattern of all is the 'St Andrews cross' pattern (Lucas & Lambin, 2005), which was the key to the solution of the structure of deoxyribonucleic acid (DNA) (Watson & Crick, 1953). This diffraction pattern was obtained by the scattering of X-rays by fibers of DNA, which may be regarded as bundles of DNA molecules with aligned molecular axes, but random orientations about this axis, and random displacements along this axis. Such a diffraction pattern may be regarded as arising from an average of diffraction patterns due to all possible azimuthal orientations of a single constituent molecule. Unlike most crystallographic work, where data from a large number of diffraction patterns from various orientations of the sample have to be combined to reconstruct the object in three dimensions (see *e.g.* Drenth, 1994; Shneerson *et al.*, 2008; Fung *et al.*, 2009), the essential elements of the three-dimensional structure of DNA were deduced from this single diffraction pattern.

The aim of the present paper is to show that, for particles with a high degree of rotational symmetry about the alignment axis, the azimuthal projection of an isolated molecule may also be deduced from a single diffraction pattern consisting of an incoherent sum of diffraction patterns of random orientations about a single axis. This is relevant to the use of laser alignment of molecules in diffraction experiments as proposed by Spence *et al.* (2005), and recently demonstrated for electron diffraction (Reckenthaeler *et al.*, 2009). If a single linearly polarized laser is used for molecular alignment, the molecules may differ in azimuthal angle about the alignment axis. The same would be true of a symmetric rotor, such as carbontrifluorobromine, CF_3Br, regardless of the state of laser polarization (Larsen *et al.*, 2000; Ho & Santra, 2008; Ho *et al.*, 2009).

The resulting composite diffraction pattern will then be similar in character to a fiber diffraction pattern. However, unlike the helices mostly studied in fiber diffraction, the individual molecules will not have the periodicity afforded by the helical pitch P. Consequently, such diffraction patterns will not manifest layer lines, and would be expected to be diffuse in all directions. This will allow an iterative phasing algorithm, which alternately modifies the magnitudes of the azimuthally projected electron density in real space and the phases of scattered amplitudes in reciprocal space (Oszlányi & Sütő, 2004, 2005), to reconstruct the azimuthally projected electron density of the particle in the case of a particle of a high degree of rotational symmetry about the alignment axis.

2. Diffraction from identical molecules of random azimuthal orientation

In this section we derive from first principles the relationship between the electron density of each particle and the composite diffraction pattern produced by the incoherent superposition of diffraction patterns of multiple copies of the particle, differing only in their azimuthal orientations. This is distinct from parallel derivations in the field of fiber diffraction (Cochran *et al.*, 1952; Franklin & Gosling, 1953*a*,*b*; Waser, 1955; Franklin & Klug, 1955; Klug *et al.*, 1958) which all

assume objects periodic along the direction of the fiber axis, which give rise to layer lines. Nevertheless, in order to draw analogies with the field of fiber diffraction, reciprocal space is specified by the three cylindrical coordinates (R, ψ, ζ), where R is the coordinate perpendicular to the molecular alignment axis (analogous to the fiber axis in fiber diffraction), ζ is that parallel to this axis, and ψ is an angular coordinate about the alignment axis (*e.g.* Cochran *et al.*, 1952; Millane & Dorset, 2001), and we make comparisons with the corresponding expressions in fiber diffraction in notes enclosed in square brackets.

A structure factor of a molecule is a function of the positions of its constituent atoms and of a scattering vector $\mathbf{q}$ in reciprocal space. Suppressing, for the moment, its dependence on the atomic coordinates, it could be expressed in terms of cylindrical reciprocal-space coordinates (R, ψ, ζ) as

$$F(R, \psi, \zeta) = \sum_m G_m(R, \zeta) \exp(im\psi). \tag{1}$$

The structure factor of a molecule rotated relative to this by an azimuthal angle ψ_j may be written

$$F_j(R, \psi, \zeta) = \sum_m G_m(R, \zeta) \exp\big[im\big(\psi - \psi_j\big)\big]. \tag{2}$$

Then, the scattered intensity from particle j is

$$\begin{aligned} I_j(R, \psi, \zeta) = |F_j(R, \psi, \zeta)|^2 &= \sum_m |G_m(R, \zeta)|^2 \\ &+ \sum_{m,m'} G_m(R, \zeta) G^*_{m'}(R, \zeta) \\ &\times \exp\big[i(m - m')\big(\psi - \psi_j\big)\big]. \end{aligned} \tag{3}$$

The first summation above represents the diagonal terms from taking the square modulus of (1), which do not depend on the azimuthal angles ψ, and the second (double) summation represents those from the off-diagonal terms, which do.

The total scattered intensity from the ensemble of molecules is $\sum_j I_j(R, \psi, \zeta)$. Owing to the randomness of the azimuthal origins ψ_j of the different molecules, the off-diagonal terms in (3) will average to zero. Since the diagonal terms in (3) do not depend on ψ, neither will the total scattered intensity from the ensemble, which may be written

$$I(R, \zeta) = I_0(R, \zeta) = N \sum_m |G_m(R, \zeta)|^2, \tag{4}$$

which has no dependence on the azimuthal angle ψ (in the above equation, N is the number of molecules in the ensemble). In other words, the scattered intensity of the molecular ensemble is cylindrically symmetric in reciprocal space. [Note that the corresponding intensity $I_l(R)$ of the layer line l in fiber diffraction is written (Millane & Dorset, 2001)

$$I_l(R) = \sum_n |G_{nl}(R)|^2, \tag{5}$$

where $G_{nl}(R)$ is defined by

$$F_l(R, \psi) = \sum_n G_{nl}(R) \exp\{in[\psi + (\pi/2)]\}, \tag{6}$$

which may be compared with our equation (1). Given that m and n are dummy indices in (4) and (5), the essential difference between the usual fiber diffraction equations (5) and (6) and our equations (4) and (1) is that the discrete layer-line index l in the former equations is replaced by the continuous coordinate ζ parallel to the alignment axis in (4) and (1).]

Although the cylindrical symmetry of the intensity distribution implies that just a single cylindrical harmonic of intensity (that corresponding to $m = 0$) in the expansion

$$I(R, \psi, \zeta) = \sum_m I_m(R, \zeta) \exp(im\psi) \tag{7}$$

suffices to describe the three-dimensional intensity distribution, a full description of the same distribution requires many (in principle all) coefficients of the corresponding cylindrical harmonic expansion of the scattered *amplitudes* (although, as we shall see later, at least for molecules with a high degree of rotational symmetry about the alignment axis, this may be a highly truncated series). In order to extract structural information from the diffraction intensities $I_0(R, \zeta)$ of (7), which may be measured, it is necessary to relate this quantity to the electron density of the scattering molecule. The molecular structure factor may be written

$$F(\mathbf{q}) = (2\pi)^{-2/3} \int f(\mathbf{r}) \exp(i\mathbf{q} \cdot \mathbf{r}) \, \mathrm{d}^3\mathbf{r}. \tag{8}$$

where $f(\mathbf{r})$ is the molecular electron density and $\mathbf{q}$ is a scattering vector. We may represent the electron density by an expansion in cylindrical harmonics,

$$f(r, \varphi, z) = \sum_m g_m(r, z) \exp(im\varphi), \tag{9}$$

where $\mathbf{r} = (r, \varphi, z)$, a set of cylindrical coordinates in real space. [We use the symbols f and g here for consistency with the field of fiber diffraction (*e.g.* Millane & Dorset, 2001). Note, however, since f is usually assumed periodic in z in that field, our more general quantity $g_m(r, z)$ is replaced by $\sum_l g_{ml}(r) \exp(2\pi ilz/c)$, where l is another integer and c is the repeat distance along z. Consequently, (9) is replaced by

$$f(r, \varphi, z) = \sum_{ml} g_{ml}(r) \exp[i(m\varphi - 2\pi lz/c)] \tag{10}$$

in fiber diffraction theory.] In our case of a completely non-periodic though finite object, we may substitute (1) and (9) into (8), and deduce that

$$\begin{aligned} &\sum_m G_m(R, \zeta) \exp(im\psi) \\ &\quad = (2\pi)^{-3/2} \iiint r \, \mathrm{d}r \, \mathrm{d}z \, \mathrm{d}\varphi \sum_m g_m(r, z) \exp(im\varphi) \\ &\qquad \times \exp\{i[\zeta z + Rr\cos(\varphi - \psi)]\}. \end{aligned} \tag{11}$$

Making use of the identity (*e.g.* Cochran *et al.*, 1952)

$$\int \mathrm{d}\varphi \exp(im\varphi) \exp[iRr\cos(\varphi - \psi)] = 2\pi i^m J_m(Rr) \exp(im\psi) \tag{12}$$

to perform the integral over φ, the right-hand side of (11) could be re-written

$$(2\pi)^{-1/2} \iint r \, \mathrm{d}r \, \mathrm{d}z \sum_m g_m(r, z) \exp(im\psi) i^m J_m(Rr) \exp(i\zeta z), \tag{13}$$

and equating the coefficients of $\exp(im\psi)$ in the left-hand sides of (11) and (13) leads to the equation

$$G_m(R, \zeta) = (2\pi)^{-1/2} \iint r g_m(r, z) i^m J_m(Rr) \exp(i\zeta z)\, \mathrm{d}r\, \mathrm{d}z \quad (14)$$

relating the coefficients of the cylindrical harmonic expansions of the molecular electron density and its scattered X-ray amplitude.

From the orthogonality relations

$$\int J_m(Rr') J_m(Rr) R\, \mathrm{d}R = \frac{\delta(r' - r)}{r'}, \quad (15)$$

valid for all m, and

$$\int \exp[i\zeta(z' - z)]\, \mathrm{d}\zeta = 2\pi\delta(z - z'), \quad (16)$$

it may be seen that the inverse relation to (14) is

$$g_m(r, z) = (2\pi)^{-1/2} \iint R G_m(R, \zeta) i^{-m} J_m(Rr) \exp(-i\zeta z)\, \mathrm{d}R\, \mathrm{d}\zeta. \quad (17)$$

Equation (14) is a combination of a Fourier transform in one dimension and a Hankel transform in the other. We term this a Fourier–Hankel transform. Equation (17) represents its inverse. These coupled two-dimensional equations relate the coefficients $G_m(R, \zeta)$ of a cylindrical harmonic expansion of the scattered amplitude and those $g_m(r, z)$ of the electron density of the scatterer. These equations are analogous to the Fourier transform and its inverse, which relate an electron density and scattered amplitude in a usual scattering problem. In a case where the magnitude of $G_m(R, \zeta)$ is known, but not its phase, and where the spatial extent of $g_m(r, z)$ is finite, it would be expected that a two-dimensional iterative phasing algorithm with appropriate constraints in reciprocal and real space (*e.g.* Fienup, 1978, 1982; Elser, 2003; Oszlányi & Sütő, 2004, 2005; Marchesini *et al.*, 2003) will allow the simultaneous determination of the unknown phases and of $g_m(r, z)$.

Algorithms which iteratively apply a support constraint due to the finite diameter of a molecule to recover its electron density have been used in fiber diffraction (Makowski *et al.*, 1980; Yamashita *et al.*, 1998). More powerful would be an algorithm which simultaneously applies support constraints in the direction of z as well as r by oversampling (Miao *et al.*, 1999) the diffraction intensities in the directions of diffraction pattern coordinates R and ζ. Although it is not possible to oversample a typical fiber diffraction pattern in the ζ direction due to the presence of discrete layer lines, this limitation is non-existent in the present case of diffraction from molecules aperiodic in all directions, where the absence of layer lines gives rise to diffuse intensities in all directions and enables the use of a full two-dimensional iterative phasing algorithm of the sort referred to above.

In practice, a more stable solution was found if these equations were reformulated in terms of an areal electron density

$$\tilde{g}_m(r, z) = r g_m(r, z) \quad (18)$$

and a corresponding quantity

$$\tilde{G}_m(R, \zeta) = R G_m(R, \zeta). \quad (19)$$

The areal electron density, so defined, is an azimuthally projected electron density per unit area in a plane passing though the symmetry axis z. With these substitutions, equations (14) and (17) may be reformulated as

$$\tilde{G}_m(R, \zeta) = (2\pi)^{-1/2} R \iint \tilde{g}_m(r, z) i^m J_m(Rr) \exp(i\zeta z)\, \mathrm{d}r\, \mathrm{d}z \quad (20)$$

and

$$\tilde{g}_m(r, z) = (2\pi)^{-1/2} r \iint \tilde{G}_m(R, \zeta) i^{-m} J_m(Rr) \exp(-i\zeta z)\, \mathrm{d}R\, \mathrm{d}\zeta, \quad (21)$$

respectively. Note that the integrals along r and R are no longer strictly Hankel transforms due to the absences of the terms r and R, respectively, in the integrands. We term the resulting one-dimensional integrals modified Hankel transforms. In practice, the Fourier transforms may be replaced by a discrete fast Fourier transform (Cooley & Tukey, 1965) and the modified Hankel transforms by their discrete equivalent. [We used a *MATLAB* routine from Leutenegger (2006), based on an earlier *Fortran* program from Anderson (1979), which uses adaptive digital filtering. This is a flexible routine which allows the calculation of a traditional Hankel transform as well as what we term a modified Hankel transform by the provision of the Bessel function kernel calculated and stored in advance for speed.]

In order to test the idea, we first simulated diffraction patterns that were the average of those from random orientations of a test molecule about a single alignment axis.

3. Simulation of diffraction pattern from molecules with random orientations about an alignment axis

In terms of a system of cylindrical coordinates, the coordinates of atom k of a molecule may be specified by (r_k, φ_k, z_k). If $f_k(\mathbf{q})$ is the form factor of atom k, the structure factor of the molecule may also be written

$$\begin{aligned} F(\mathbf{q}) = F(R, \psi, \zeta) &= \sum_k f_k \exp(i\mathbf{q} \cdot \mathbf{r}_k) \\ &= \sum_k f_k \exp\{i[\zeta z_k + R r_k \cos(\varphi_k - \psi)]\}. \end{aligned} \quad (22)$$

Equating the right-hand sides of (1) and (22), multiplying both sides by $\exp(-im\psi)$, integrating with respect to ψ, and making use of the identity (12) shows that

$$G_m(R, \zeta) = \sum_k f_k \exp[i(\zeta z_k - m\varphi_k)] i^m J_m(Rr_k). \quad (23)$$

Equations (23) and (4) allow the calculation of the diffraction pattern $I_0(R, \zeta)$ from a collection of identical molecules differing only in angle of rotation about the z axis. The non-zero terms in the sum (4) will depend on the degree of rotational symmetry about this axis.

3.1. Application to a short single-wall C nanotube

For our test case, we took a short single-wall C nanotube (SWNT) with caps on both ends, as illustrated in Fig. 1. This is a molecule with five-fold rotational symmetry about the axis of

the nanotube. However, its projection along this axis has a tenfold axis of symmetry, as illustrated in Fig. 1(*b*).

The diffraction pattern from a collection of such molecules with random azimuthal orientations about the z axis, as calculated from equations (23) and (4) with atomic scattering factors calculated from the Cromer–Mann coefficients (Cromer & Mann, 1968), is shown in Fig. 2(*a*).

The electron density of an SWNT projected along the z axis is tenfold rotationally symmetric, and projection of the cylindrical harmonic expansion of its areal electron density (18) will be characterized by quantum numbers of modulo 10 only, *i.e.* $m = 0, 10, 20 \ldots$. A consequence of (20) is that the coefficients $\tilde{G}_m(R, 0)$ of the cylindrical harmonic expansion of the scattered areal amplitude in the equatorial plane $\zeta = 0$ will also be characterized by the same quantum numbers. It will be noted also that the maximum value of the argument of the Bessel function on the right-hand side of (20) will be $r_{\max}R_{\max}$, $(= x$, say), where $r_{\max}$ is the maximum radial coordinate of any atom of the molecule relative to the molecular rotation axis, and $R_{\max}$ is the maximum value of the coordinate R of the diffraction pattern. For an SWNT, $r_{\max}$ is about 3 Å and, for the simulated diffraction pattern of Fig. 3, $R_{\max}$ is 2 Å^{-1}. Thus, x $(= r_{\max}R_{\max})$ is about 6. Cochran *et al.* (1952) noted that $J_m(x)$ was negligible for values of x less than about m. Consequently, it would be expected that the contributions of $I_m(R, 0) = |G_m(R, 0)|^2$ to the diffraction pattern intensity $I(R, 0)$ would be negligible for x less than about m. Given that, in this case, x is about 6, and that the lowest permissible value of m (apart from 0) is 10, it can be concluded that $I_0(R, 0)$ is the overwhelmingly dominant contributor to $I(R, 0)$ for $R < R_{\max}$, as is indeed borne out in Fig. 1(*c*). The arguments above suggest that the intensities of the composite diffraction pattern of SWNTs differing only in azimuthal orientation about the cylinder axis (at least up to $R = R_{\max}$) might be approximated by a cylindrical harmonic expansion of the scattered amplitudes which contains just the term $m = 0$, *i.e.* that $|G_0(R, \zeta)|$ might be approximated by the square root of the intensities $I(R, \zeta)$, of the measured diffraction pattern. Of course, the phases of $G_0(R, \zeta)$ are not determined by such a procedure. However, these phases may be determined by iteratively solving (20) and (21) to convergence applying appropriate constraints in real and reciprocal space (Miao *et al.*, 1999; for a review, see Spence, 2006).

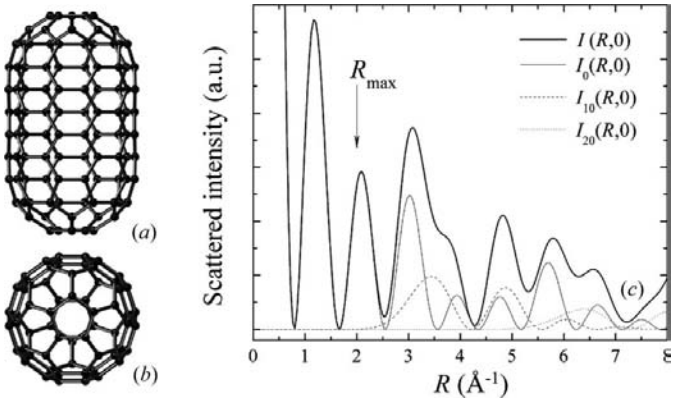

Figure 1
Schematic views of a short single-wall C nanotube, whose C—C bonds are of length ∼1.4 Å, viewed (*a*) perpendicular to and (*b*) parallel to the molecular alignment axis. Panel (*c*) depicts the total diffraction pattern intensity as a function of the reciprocal-space coordinate R for $\zeta = 0$, as well as the magnitudes of the contributions from the $m = 0$, 10 and 20 cylindrical harmonics. $R_{\max}$ (= 2 Å^{-1}) indicates the maximum value of R corresponding to the edge of the simulated diffraction pattern in Fig. 3(*a*). The present figure shows that, up to $R = R_{\max}$ (corresponding to $2\pi/R_{\max}$ $\simeq$ 3 Å resolution), there is negligible error in modeling $I(R, 0)$ by just the $m = 0$ component.

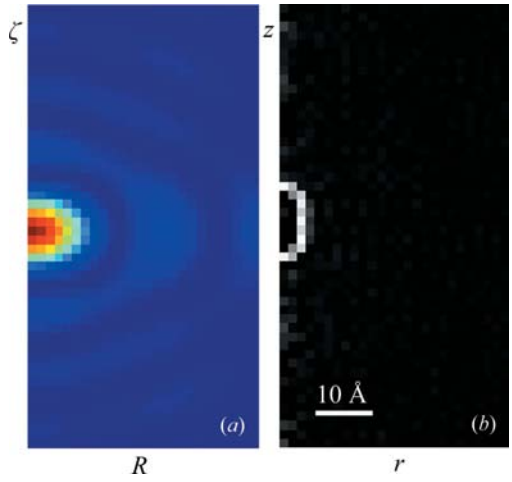

Figure 2
(*a*) Simulation of the diffraction pattern expected from a sum of those of a short SWNT of all azimuthal orientations about its axis (assumed perpendicular to the incident X-rays). The reciprocal-space coordinate parallel to the SWNT axis is denoted by ζ, while R is that perpendicular to ζ. The simulation assumes a flat Ewald sphere. The maximum values of R and $|\zeta|$ are 2 Å^{-1}, corresponding to a real-space resolution of about 3 Å. (*b*) Azimuthal projection of the electron density of the SWNT on a plane perpendicular to the tube axis, as reconstructed from the diffraction pattern in (*a*) by the algorithm described in the paper.

3.2. Tests of the two-dimensional phasing algorithm

The iterations were initiated by assigning in equation (21) random phases (consistent with Friedel's rule for a real

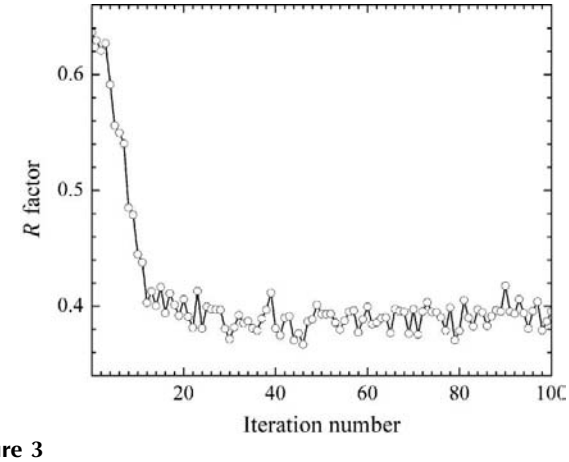

Figure 3
Variation of the R factor, equation (24), monitoring the degree of agreement between the simulated diffraction pattern and its current estimate from the iterative reconstruction algorithm, as a function of iteration number.

projected areal electron density) to $|\tilde{G}_0(R, \zeta)|$ {whose magnitude was taken to be $R[I_0(R, \zeta)]^{1/2}$}. Evaluation of (21) gave an initial estimate of the areal electron density $\tilde{\rho}_0(r, z)$. The standard deviation, σ, of this distribution was evaluated, and the distribution subsequently modified according to the *charge flipping* prescription of Oszlányi & Sütő (2008), namely, the signs of the densities whose values were below $\alpha\sigma$ in magnitude were flipped (where α was taken to be 0.7), *i.e.* the positive densities were made negative, and the negative densities positive if their values were below this threshold.

Application of the inverse transform (20) then produced a calculated estimate of the (complex) amplitudes $\tilde{G}_0(R, \zeta)$. For the largest 80% of the amplitudes, their magnitudes were replaced by their known 'experimental' values, while retaining the calculated phases. For the smallest 20%, their magnitudes were accepted unaltered, but their phases were 'shifted' by $\pi/2$ radians (Oszlányi & Sütő, 2005). This sequence of steps was then iterated, and convergence was monitored by means of the reliability factor (R factor)

$$R_f = \sum_{j,k} \Big\{ \big| |\tilde{G}_0^{(\exp)}(R_j, \zeta_k)| / \sum_{j',k'} |\tilde{G}_0^{(\exp)}(R_{j'}, \zeta_{k'})| - |\tilde{G}_0(R_j, \zeta_k)| / \sum_{j',k'} |\tilde{G}_0(R_{j'}, \zeta_{k'})| \big| \Big\} \quad (24)$$

between the current estimate of $|\tilde{G}_0(R_j, \zeta_k)|$ at pixels (j, k) and their corresponding 'experimental' values $|\tilde{G}_0^{(\exp)}(R_j, \zeta_k)|$ estimated from the simulated $I(R_j, \zeta_k)$, as suggested by Oszlányi & Sütő (2008). The calculated R factor as a function of iteration number in our simulations is shown in Fig. 3. The R factor falls with increasing iteration number until about 20 iterations, and then remains approximately constant, suggesting convergence. It should be noted that this algorithm makes no assumptions about the size of the object, as no 'support' constraint was assumed.

The final image resulting from the iterative phasing algorithm is shown in Fig. 2(*b*) (any remaining negative values in the final image were set to zero). The azimuthal projection of the SWNT onto a plane perpendicular to the tube axis is clearly visible in this image.

The charge flipping algorithm has been applied here to a non-periodic object, unlike the crystalline objects for which it was developed, which do not provide oversampling and which therefore require atomic resolution data. Another application of the flipping algorithm has been described by Wu *et al.* (2004), who showed it to be equivalent to the *output-output* algorithm of Fienup (1982) with feedback parameter $\beta = 2$.

4. Discussion

These results apply to diffraction from many molecules with single-axis alignment and no periodicity along that axis. We assume no coherent interference between different molecules, and random azimuthal orientations. As such, the treatment is applicable directly to laser alignment schemes (Spence *et al.*, 2005; Reckenthaeler *et al.*, 2009), and other sample preparation methods (such as flow alignment, alignment in gels, alignment in electric and magnetic fields *etc.*) which impose single-axis alignment. If plane-wave laser alignment is used, the minimum energy orientation is degenerate, and molecules may be erect or inverted in the laser beam. This degeneracy must be combined with the enantiomorphous ambiguity which results from Friedel symmetry in the diffraction pattern. The results are discussed elsewhere (Spence *et al.*, 2005; Elser & Millane, 2008), where it is shown that these ambiguities do not prevent solution of the phase problem. If elliptical laser light is used for alignment, the direction (but not the sense) of all three Cartesian axes of the polarizability may be fixed, and similar considerations apply. Simulations of the effects of imperfect alignment on resolution have been published elsewhere (Spence *et al.*, 2005). For the case of the simulations reported here, an obvious conservative estimate of tolerable misalignment (in radians) is the ratio of the size ΔR of a diffraction pattern pixel to the resolution, $R_{\max}$. In the case of our simulation for a C nanotube, this ratio is 1/25 radians, or 2.3°.

5. Conclusions

The theory of fiber diffraction is generally applied to fibers of elongated molecules, often of helical structure, with a repeat distance P along the helical axis. This gives rise to a periodicity along this direction, whose most visible manifestation on fiber diffraction patterns, *e.g.* the famous 'St Andrews cross' pattern of DNA, are 'layer lines' separated in reciprocal space by $1/P$.

The composite diffraction pattern from an incoherent superposition of those from a set of isolated molecules is devoid of translational periodicity even if all molecules are aligned parallel to a single molecular axis. The resulting lack of translational periodicity results in their diffraction patterns being completely diffuse with no Bragg spots or layer lines. The average of the diffraction patterns from all azimuthal orientations of the individual molecules is likewise diffuse, or continuous.

At least for molecules with a high degree of rotational symmetry about the alignment axis, we have shown that it is possible to deduce the azimuthal projection of the electron density of each molecule from such composite diffraction patterns. In such a case, the square root of the measured intensity is a good approximation to the magnitude of the azimuthally averaged scattered amplitude. This in turn is related to the azimuthally averaged electron density by a two-dimensional transform, which is a Fourier transform in the molecular alignment direction, and a Hankel transform in the direction perpendicular to this. If we term this a Fourier–Hankel transform, an inverse Fourier–Hankel transform relates the azimuthally averaged electron density to the azimuthally averaged amplitude.

Since the phases of the scattered amplitudes cannot be deduced directly from measured intensities, they need to be found by iterations of the Fourier–Hankel transform and its inverse, applying a constraint of the known magnitudes of the amplitudes in reciprocal space and some sort of density modification in real space analogous to methods in use for a scattered amplitude and electron density related by a multi-

dimensional Fourier transform and its inverse. However, to our knowledge, the application of such an iterative phasing algorithm to Fourier–Hankel transforms is new, and a significant extension of such phasing and inverse methods.

We thank Abbas Ourmazd and Robin Santra for helpful discussions, and Michael Treacy for providing the atomic coordinates of a short single-wall C nanotube. We acknowledge financial support from the US Department of Energy (grant Nos. DE-SC0003141 and DE-FG02-06ER46277).

References

Anderson, W. L. (1979). *Geophysics*, **44**, 1287–1305.
Cochran, W., Crick, F. H. & Vand, V. (1952). *Acta Cryst.* **5**, 581–586.
Cooley, J. W. & Tukey, J. W. (1965). *Math. Comput.* **19**, 297–301.
Cromer, D. T. & Mann, J. B. (1968). *Acta Cryst.* A**24**, 321–324.
Drenth, J. (1994). *Principles of Protein X-ray Crystallography*. New York: Springer-Verlag.
Elser, V. (2003). *J. Opt. Soc. Am. A*, **20**, 40–55.
Elser, V. & Millane, R. P. (2008). *Acta Cryst.* A**64**, 273–279.
Fienup, J. R. (1978). *Opt. Lett.* **3**, 27–29.
Fienup, J. R. (1982). *Appl. Opt.* **21**, 2758–2769.
Franklin, R. E. & Gosling, R. G. (1953*a*). *Acta Cryst.* **6**, 678–685.
Franklin, R. E. & Gosling, R. G. (1953*b*). *Nature (London)*, **171**, 740–741.
Franklin, R. E. & Klug, A. (1955). *Acta Cryst.* **8**, 777–780.
Fung, R., Shneerson, V. L., Saldin, D. K. & Ourmazd, A. (2009). *Nat. Phys.* **5**, 64–67.
Ho, P. J. & Santra, R. (2008). *Phys. Rev. A*, **78**, 053409.
Ho, P. J., Starodub, D., Saldin, D. K., Shneerson, V. L., Ourmazd, A. & Santra, R. (2009). *J. Chem. Phys.* **131**, 131101.
Klug, A., Crick, F. H. C. & Wyckoff, H. W. (1958). *Acta Cryst.* **11**, 199–213.
Larsen, J. J., Hald, K., Bjerre, N. & Stapelfeldt, H. (2000). *Phys. Rev. Lett.* **85**, 2470–2473.
Leutenegger, M. (2006). *MATLAB Toolbox*, http://wwwuser.gwdg.de/~mleuten/MATLABToolbox/HankelTransform.html.
Lucas, A. A. & Lambin, P. (2005). *Rep. Prog. Phys.* **68**, 1181–1249.
Makowski, L., Caspar, D. L. D. & Marvin, D. A. (1980). *J. Mol. Biol.* **140**, 149–181.
Marchesini, S., He, H., Chapman, H. N., Hau-Riege, S. P., Noy, A., Howells, M. R., Weierstall, U. & Spence, J. C. H. (2003). *Phys. Rev. B*, **68**, 140101(R).
Miao, J., Charalambous, P., Kirz, J. & Sayre, D. (1999). *Nature (London)*, **400**, 342–344.
Millane, R. P. & Dorset, D. L. (2001). *International Tables for Crystallography*, Vol. B, 2nd ed., pp. 466–485. Dordrecht: Kluwer Academic Publishers.
Oszlányi, G. & Sütő, A. (2004). *Acta Cryst.* A**60**, 134–141.
Oszlányi, G. & Sütő, A. (2005). *Acta Cryst.* A**61**, 147–152.
Oszlányi, G. & Sütő, A. (2008). *Acta Cryst.* A**64**, 123–134.
Reckenthaeler, P., Centurion, M., Fuss, W., Trushin, S. A., Krausz, F. & Fill, E. E. (2009). *Phys. Rev. Lett.* **102**, 213001.
Shneerson, V. L., Ourmazd, A. & Saldin, D. K. (2008). *Acta Cryst.* A**64**, 303–315.
Spence, J. C. H. (2006). *Lensless Imaging*. In *Science of Microscopy*. New York: Springer.
Spence, J. C. H., Schmidt, K., Wu, J. S., Hembree, G., Weierstall, U., Doak, B. & Fromme, P. (2005). *Acta Cryst.* A**61**, 237–245.
Waser, J. (1955). *Acta Cryst.* **8**, 142–150.
Watson, J. D. & Crick, F. H. C. (1953). *Nature (London)*, **171**, 737–738.
Wu, J. S., Weierstall, U., Spence, J. C. H. & Koch, C. T. (2004). *Opt. Lett.* **29**, 2737–2739.
Yamashita, I., Hasegawa, K., Suzuki, H., Vonderviszt, F., Mimori-Kiyosue, Y. & Namba, K. (1998). *Nat. Struct. Biol.* **5**, 125–132.